



OPEN

SUBJECT AREAS:
ELECTRONIC MATERIALS
BATTERIESReceived
28 October 2014Accepted
23 January 2015Published
23 February 2015Correspondence and
requests for materials
should be addressed to
W.-Y.L. (iamwylai@
njupt.edu.cn); H.P.
(huanpangchem@
hotmail.com) or W.H.
(iamwhuang@njupt.
edu.cn)

Room temperature synthesis of cobalt-manganese-nickel oxalates micropolyhedrons for high-performance flexible electrochemical energy storage device

Yi-Zhou Zhang¹, Junhong Zhao², Jing Xia², Lulu Wang², Wen-Yong Lai¹, Huan Pang^{1,2,3} & Wei Huang¹

¹Key Laboratory for Organic Electronics & Information Displays (KLOEID), Institute of Advanced Materials (IAM), National Jiangsu Synergetic Innovation Center for Advanced Materials (SICAM), Nanjing University of Posts and Telecommunications (NUPT), Nanjing, 210023, China, ²Key Laboratory for Clearer Energy and Functional Materials of Henan Province, College of Chemistry and Chemical Engineering, Anyang Normal University, Anyang, 455000, China, ³State Key Laboratory of Coordination Chemistry, Nanjing University, Nanjing, 210093, China.

Cobalt-manganese-nickel oxalates micropolyhedrons were successfully fabricated by a room temperature chemical co-precipitation method. Interestingly, the $\text{Co}_{0.5}\text{Mn}_{0.4}\text{Ni}_{0.1}\text{C}_2\text{O}_4 \cdot n\text{H}_2\text{O}$ micropolyhedrons and graphene nanosheets have been successfully applied as the positive and negative electrode materials (a battery type Faradaic electrode and a capacitive electrode, respectively) for flexible solid-state asymmetric supercapacitors. More importantly, the as-assembled device achieved a maximum energy density of $0.46 \text{ mWh} \cdot \text{cm}^{-3}$, a decent result among devices with similar structures. The as-assembled device showed good flexibility, functioning well under both normal and bent conditions (0° – 180°). The resulting device showed little performance decay even after 6000 cycles, which rendered the $\text{Co}_{0.5}\text{Mn}_{0.4}\text{Ni}_{0.1}\text{C}_2\text{O}_4 \cdot n\text{H}_2\text{O} // \text{Graphene}$ device configuration a promising candidate for high-performance flexible solid-state asymmetric supercapacitors in the field of high-energy-density energy storage devices.

High-performance energy conversion-storage devices have been receiving a lot of research attention recently^{1–5}. Electrochemical capacitors, also known as supercapacitors (SCs), are widely regarded as suitable candidates for the next generation power source owing to their high power density, high stability and low fabrication cost^{6,7}. SCs are widely applied in many fields such as emergency power supplies, electronic devices, and hybrid-electric machines. However, the energy density of SCs are generally not high enough to be used as sustainable power sources for many applications. Much effort has been devoted to improving the energy density of SCs. One promising strategy is to design nanostructured electrode materials with a large amount of active sites and high structural stability. Various micro/nanomaterials including nanoparticles⁸, nanowires^{9,10}, nanotubes¹¹ and nanosheets^{12,13} have been successfully applied as SC electrodes with high energy density. On the other hand, solid-state asymmetric supercapacitors (SASCs) comprising a battery type Faradaic electrode as an energy source and a capacitive electrode as a power source are promising alternatives to conventional SCs which are symmetrical using liquid electrolytes^{14–18}. SASCs using solid-state electrolytes can avoid the potential problem of electrolyte leakage and are more environmentally friendly. What's more, compared with conventional SCs, SASCs have other advantages including light-weight, small-size, good reliability, ease of handling, and a wider of operating temperature range^{19,20}, making SASCs suitable for wearable and flexible electronics. As an example, Lu et al have successfully reported a SASC based on $\text{MnO}_2 // \text{Fe}_2\text{O}_3$ nanowires²¹. However, it still remains a great challenge to fabricate high-performance SASCs.

Transition metal oxalate micro/nano materials have been recently explored as precursors for the synthesis of porous transition metal oxides (NiO ^{22,23}, Mn_2O_3 ²², CeO_2 ²⁴ and so on) and porous mixed transition metal oxides (NiMn_2O_4 ²⁵, $\text{Ni}_{0.3}\text{Co}_{2.7}\text{O}_4$ ^{26,27}, ZnO-NiO ²⁸, Co-Ni-Mn oxide nanowires²⁹ and so on). As a matter of fact, however, metal oxalates themselves can be used as electrode materials. Compared with the synthesis of traditional metal



oxides, the synthesis of the metal oxalates generally involves only simple synthetic methods in aqueous solution (usually, a simple and scalable co-precipitation method under room temperature) thus the materials are obtained with low cost, environmental friendliness and safety. Micro/nanostructural nickel oxalates are an interesting class and have been successfully applied to make electrodes for electrochemical capacitors³⁰ and asymmetric supercapacitors³¹.

In this work, we have successfully synthesized uniform cobalt-manganese-nickel oxalates ($\text{Co}_{0.5}\text{Mn}_{0.4}\text{Ni}_{0.1}\text{C}_2\text{O}_4 \cdot n\text{H}_2\text{O}$) micropolyhedrons by a room temperature chemical co-precipitation method. The synthesis method is green with low energy consumption. More importantly, $\text{Co}_{0.5}\text{Mn}_{0.4}\text{Ni}_{0.1}\text{C}_2\text{O}_4 \cdot n\text{H}_2\text{O}$ micropolyhedrons can be successfully used as the positive electrode materials for SASCs (graphene nanosheets as the negative electrode material). A maximum energy density of $0.46 \text{ mWh} \cdot \text{cm}^{-3}$ was obtained easily by the as-assembled SASC, which was higher than most of previous results. The good flexibility of the as-assembled SASC device enabled it to work under both the normal and the bent condition (0° – 180°). An efficiency cycle ability was found after 6000 cycles, which made $\text{Co}_{0.5}\text{Mn}_{0.4}\text{Ni}_{0.1}\text{C}_2\text{O}_4 \cdot n\text{H}_2\text{O}$ /Graphene SASC a promising candidate for high-performance flexible SASC in the field of high-energy-density energy storage devices.

Results

$\text{Co}_{0.5}\text{Mn}_{0.4}\text{Ni}_{0.1}\text{C}_2\text{O}_4 \cdot n\text{H}_2\text{O}$ micropolyhedrons were obtained by a room temperature chemical co-precipitation condition (See experimental section). The XRD patterns of the as-prepared samples are shown in Figure 1. In view of the single oxalate phases (JCPDS#01-0296-cobalt oxalate hydrate, JCPDS#01-0283-manganese oxalate

hydrate and JCPDS#01-0299-nickel oxalate hydrate), all the peaks of the as-prepared product are from the coupling result of three phases, which could not be indexed to a single oxalate. It indirectly indicates that the mixed oxalates have formed. Figure 1b,c show the typical SEM images of the as-prepared sample, and the uniform micropolyhedron with $10 \mu\text{m}$ was the main product. To identify the correct element ratio of the as-prepared sample, EDS-Mapping has been measured (Figure 1e–g). The contrast of light-shade intensity is related with the element content. Clearly, the order of the element content is $\text{Co} > \text{Mn} > \text{Ni}$ from the results of Figure 1e–g. And the detailed quantitative calculation is also shown in Figure S1: C 12.0%, O 54.2%, Mn 12.1%, Co 16.2%, Ni 3.2%. The three metal element atom ratio is $\text{Co}:\text{Mn}:\text{Ni} = 5:4:1$, which is highly consistent with the raw material ratio. Additionally, Co, Mn and Ni contents were analyzed by ICP-OES (PE-3300DV) after the sample was dissolved. The ICP result confirmed the three element atom ratio was $\text{Co}:\text{Mn}:\text{Ni} = 5:4:1$, consistent with the EDS result.

Discussion

The electrochemical property of the as-prepared $\text{Co}_{0.5}\text{Mn}_{0.4}\text{Ni}_{0.1}\text{C}_2\text{O}_4 \cdot n\text{H}_2\text{O}$ electrode was first studied in the three electrode configuration by Cyclic Voltammetry (CV) and Chronopotentiometry (CP) measurements (Figure 2). From Figure 2a and Figure S2, unlike the shape of electric double-layer capacitance, CV curves suggested that the electrochemical capacity was mainly pseudocapacitive. What's more, the Faradaic pseudocapacitive characteristics may result from the redox mechanism of the surface metal ion. A reversible redox reaction was proposed to occur on the as-prepared electrode:

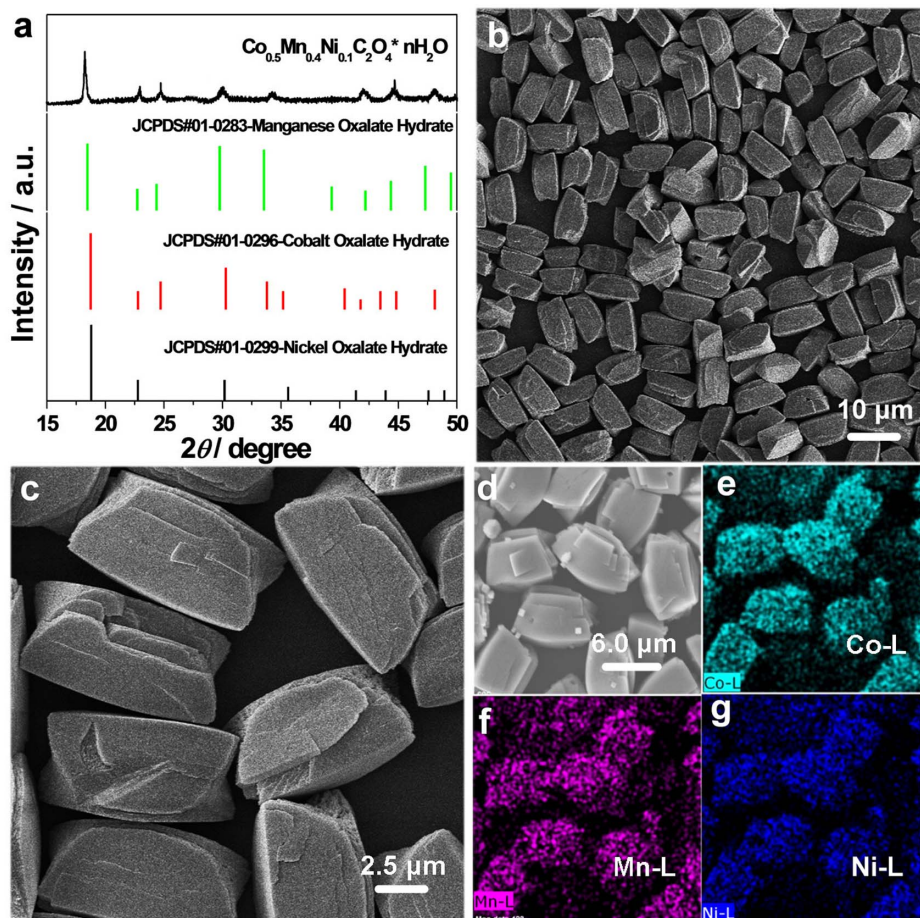


Figure 1 | (a) XRD patterns of as-prepared samples, JCPDS#01-0296-cobalt oxalate hydrate, JCPDS#01-0283-manganese oxalate hydrate and JCPDS#01-0299-nickel oxalate hydrate; (b–d) SEM images, and (e–g) EDS-mapping images for different elements.

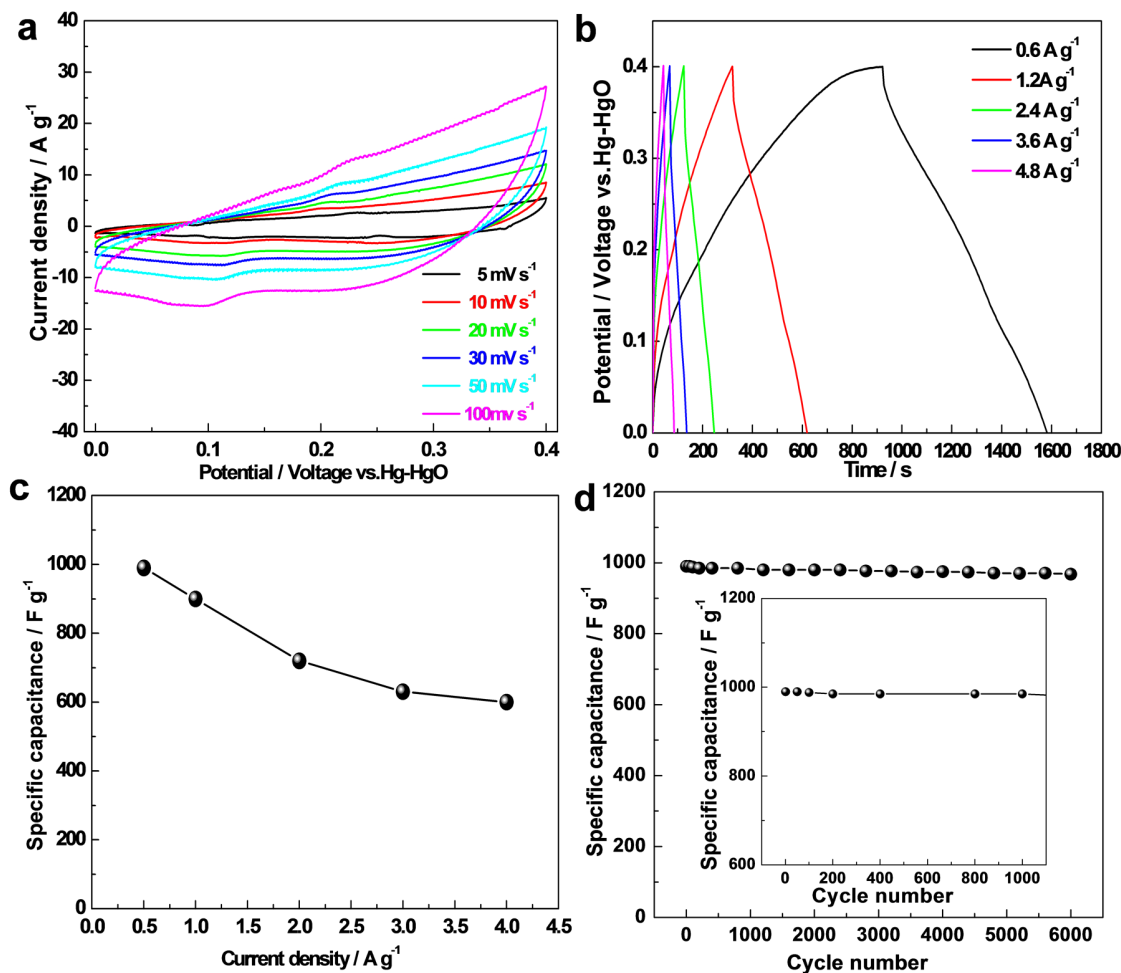
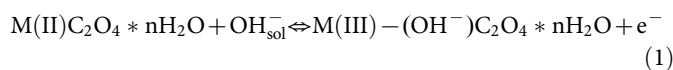


Figure 2 | In a three-electrode system in 3.0 M KOH solution. (a) CV curves with different scan speeds; (b) CP curves with different current densities; (c) Specific capacitance calculated based on the discharge curve from (b), and (d) Cycling life test at 0.6 A g⁻¹.



CP curves of the as-prepared electrode with different current densities are shown in Figure 2b. Clearly, the discharge time decreased with the increase of current density. However, it exhibited rather high electrode polarization even at low current densities as shown in Figure 2b, we thus supposed that irreversible reactions happened. The specific capacitances calculated from the discharging curves with different current densities are shown in Figure 2c. The specific capacitances achieved 990 F g⁻¹ at 0.6 A g⁻¹, and 600 F g⁻¹ at even 4.0 A g⁻¹ in 3.0 M KOH solution. Interestingly, the as-prepared electrode exhibited stable cycling performance with a specific capacitance of 968 F g⁻¹ even after 6000 cycles (Figure 2d). Clearly, the as-prepared electrode showed no capacity decay after 1000 cycles in the inset of Figure 2d, further confirming the pragmatic value of the Co_{0.5}Mn_{0.4}Ni_{0.1}C₂O₄·nH₂O electrode.

The graphene electrode in three-electrode system have been evaluated. As depicted in Figure S3, the graphene electrode shows a good specific capacitance (277 F g⁻¹, 0.6 A g⁻¹) which also offers a good cycle life (88.8%, Retention 10000 cycle).

We have successfully assembled a SASC device using Co_{0.5}Mn_{0.4}Ni_{0.1}C₂O₄·nH₂O micropolyhedrons and graphene nanosheets. To measure the electrochemical property of the as-prepared device, CV and CP measurements were tested carefully. Unlike the three-electrode electrochemical feature, the SASC device displayed a quasi-rectangular CV geometry with feeble redox peaks, indicating a

combination of both pseudocapacitive and electric double-layer capacitor properties at all scan rates in Figure 3a. Moreover, galvanostatic charge-discharge curves of the as-prepared device with different current densities (0.50–4.0 mA cm⁻²) are shown in Figure 3b. The good symmetry of curves showed excellent reversibility of the as-prepared device. The linear sloping of galvanostatic charge-discharge curves is not only characteristic of EDLC, but also of the combination the pseudocapacitive behavior with EDLC behavior. In other word, the electrochemical property of the SASC device results from the combination of a battery type Faradaic electrode and a capacitive electrode. The largest specific capacitance of the as-prepared device can reach up to 86.3 mF cm⁻² at a current density of 0.50 mA cm⁻², 55 mF cm⁻² at 4.0 mA cm⁻² in Figure 3c. In order to test the flexibility of the as-prepared device, the SASC was bended with different angles (0°, 30°, 90°, and 180°, Inset-corresponding optical images), while corresponding CV tests were carried out (Figure 3d). Remarkably, throughout the bending processes, the shape of CV curve was nearly unchanged, suggesting good flexibility of the device. In fact, we have measured the performance of as-prepared device after 400 bending times as depicted in Figure S4. The as-prepared device showed only 0.1% performance decay after 400 bendings. The SASC maintained 98.6% of the initial specific capacitance after 2000 cycles and at least 98.6% after 6000 cycles as shown in Figure 3e. The stable cycling performance is much better than most previous results, such as PANI/CNT//PANI/CNT (88.6% after 1000 cycles)¹⁷, MnO₂ NW/graphene//graphene (79% after 1000 cycles)³², and RuO₂-graphene//graphene (95% after 2000 cycles)³³. In

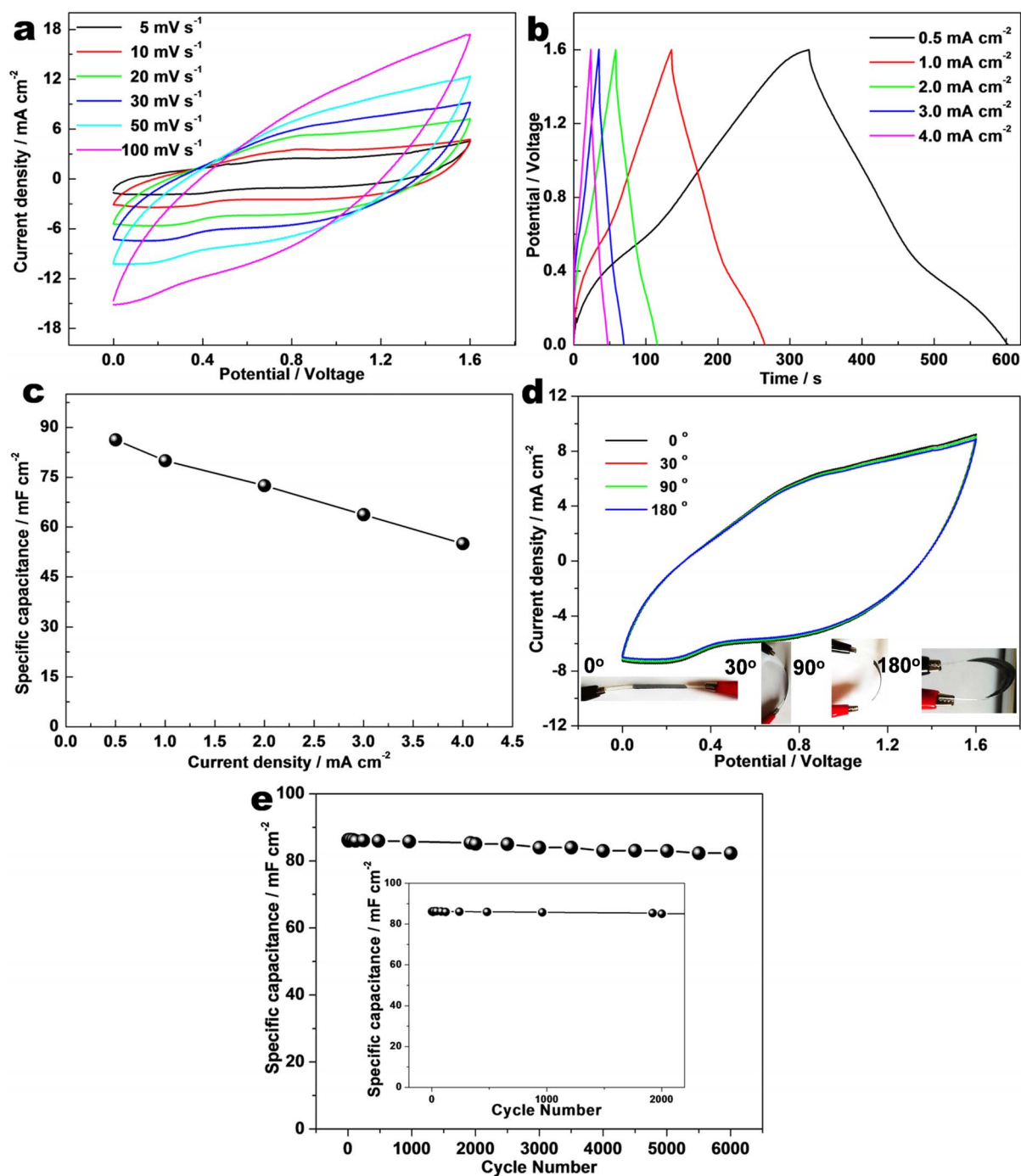


Figure 3 | (a) Cyclic voltammetry of the as-prepared SASC device with different scan rate from 5 to 100 mV s^{-1} ; (b) The galvanostatic charge-discharge curves with different current densities, 0.50–4.0 mA cm^{-2} ; (c) Corresponding specific capacitance calculated by discharge curves in (b); (d) CV curves at a scan rate 30 mV s^{-1} with different bended degrees (0° , 30° , 90° and 180° , Inset-corresponding optical images), and (e) Cycle life testing at 0.5 mA cm^{-2} for 6000 cycles, and 2000 cycles-Inset.

addition, the electrochemical impedance spectroscopy (EIS) analysis before and after the cycling are compared in Figure S5. From the EIS result in Figure S5, the resistance only changed slightly, which further confirms the stability of the electrochemical performance.

The volumetric energy and power densities of the as-prepared flexible SASC calculated based on the data in Figure 3b are shown in Figure 4. For comparison, the volumetric power and energy densities of other energy storage devices are also plotted. The as-fabricated flexible SASC possessed a maximum volumetric energy density of $0.46 \text{ mW}\cdot\text{h}\cdot\text{cm}^{-3}$ at $0.5 \text{ mA}\cdot\text{cm}^{-2}$, and $0.29 \text{ mW}\cdot\text{h}\cdot\text{cm}^{-3}$ at $4.0 \text{ mA}\cdot\text{cm}^{-2}$, also showing good rate performance of the flexible

SASC device. Moreover, the maximum volumetric energy density of the as-prepared flexible SASC was considerably higher in comparison with those of recently reported devices^{9a,18,21,34–37,39,40}, such as $\text{TiO}_2@\text{MnO}_2/\text{TiO}_2/\text{C}$ ($0.5 \text{ mA}\cdot\text{cm}^{-2}$ – $0.30 \text{ mW}\cdot\text{h}\cdot\text{cm}^{-3}$)¹⁸, $\text{MnO}_2//\text{Fe}_2\text{O}_3$ ($0.5 \text{ mA}\cdot\text{cm}^{-2}$ – $0.41 \text{ mW}\cdot\text{h}\cdot\text{cm}^{-3}$)²¹ and $\text{ZnO}@\text{MnO}/\text{Graphene}$ ($0.5 \text{ mA}\cdot\text{cm}^{-2}$ – $0.234 \text{ mW}\cdot\text{h}\cdot\text{cm}^{-3}$)³⁹. However, the obtained maximum volumetric energy density was lower than those from ref. 9b, 15, 38, 41 and 42. Additionally, the SASC device can offer a maximum power density of $46 \text{ mW}\cdot\text{cm}^{-3}$ at $4.0 \text{ mA}\cdot\text{cm}^{-2}$, which is much higher than that of recently reported $\text{ZnO}@\text{MnO}_2$ ³⁷, polyaniline// $\text{WO}_x@$ MoO_x ³⁸, and $\text{ZnO}@\text{MnO}_2//\text{Graphene}$ ³⁹, and NiO/C ⁴⁰, but lower than

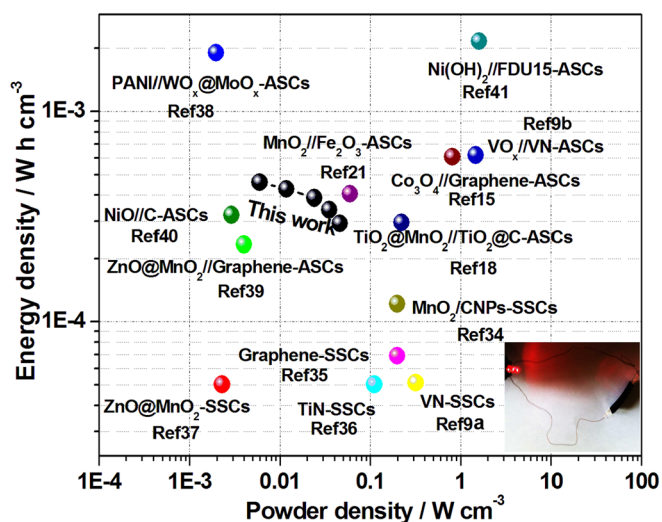


Figure 4 | Ragone plots of the as-prepared SASC device. The values reported for other previous devices are added for comparison^{9,15,18,21,34–41}. Inset shows a red LED (1.5 V) powered by the as-prepared SASC.

that of other devices^{9b,15,18,21,34–36,41,42}. The results above confirmed that the $\text{Co}_{0.5}\text{Mn}_{0.4}\text{Ni}_{0.1}\text{C}_2\text{O}_4 \cdot n\text{H}_2\text{O}$ micropolyhedron is a promising anode material for SASCs. To demonstrate the potential application of the as-prepared ASC device, an ASC device was employed to power a red light-emitting-diode (LED) as shown in the inset of Figure 4. The ASC device can power a red LED (1.5 V) for about 2 min after charging at 0.5 mA cm^{-2} for 30 s.

We attribute the excellent electrochemical energy storage behavior to the desirable synergy of composition and nanostructure of as-prepared materials. Specifically, the primary nanopores (Figure S6) provide high electrochemical activity and relatively high active surface area ($89 \text{ m}^2 \text{ g}^{-1}$), while the secondary micropolyhedrons in micrometer dimensions prevent the undesirable agglomeration and ensure the stability of the porous structure. It is worth mentioning that the abundant mesopores are of great significance for the electrochemical processes.

In summary, $\text{Co}_{0.5}\text{Mn}_{0.4}\text{Ni}_{0.1}\text{C}_2\text{O}_4 \cdot n\text{H}_2\text{O}$ micropolyhedron has been successfully synthesized *via* a room temperature chemical coprecipitation method. More importantly, a flexible SASC device has been successfully constructed with using the resulting $\text{Co}_{0.5}\text{Mn}_{0.4}\text{Ni}_{0.1}\text{C}_2\text{O}_4 \cdot n\text{H}_2\text{O}$ micropolyhedrons and graphene nanosheets. The assembled $\text{Co}_{0.5}\text{Mn}_{0.4}\text{Ni}_{0.1}\text{C}_2\text{O}_4 \cdot n\text{H}_2\text{O}/\text{graphene}$ SASC achieved a maximum energy density of $0.46 \text{ mWh} \cdot \text{cm}^{-3}$, which was higher than most of the reported solid state SCs. The resulting SASC exhibited excellent efficiency cycle stability for 6000 cycles, which rendered it as one of the top high-performance flexible solid-state asymmetric supercapacitors. Other applications are anticipated by fully exploiting the advantages of flexibility and high energy density originated from both the materials architecture and the novel design of the device. Further work is undergoing in our lab to improve the device performance and to extend the philosophy in this work into other systems within the framework of flexible/stretchable energy devices.

Methods

Synthesis of the $\text{Co}_{0.5}\text{Mn}_{0.4}\text{Ni}_{0.1}\text{C}_2\text{O}_4 \cdot n\text{H}_2\text{O}$ micropolyhedron. All of the chemical reagents were of analytical grade and used without further purification. In a typical preparation, 10.0 mL 0.10 M $\text{Co}(\text{CH}_3\text{COO})_2$ -ethylene glycol solution, 8.0 mL 0.10 M $\text{Mn}(\text{CH}_3\text{COO})_2$ -ethylene glycol solution and 2.0 mL 0.10 M $\text{Ni}(\text{CH}_3\text{COO})_2$ -ethylene glycol solution were mixed and stirred for 10 min. Then 40.0 mL 0.10 M $(\text{NH}_4)_2\text{C}_2\text{O}_4 \cdot \text{H}_2\text{O}$ solution was added into the above solution, and then mixed vigorously for 2 h, and the resulting mixture was incubated at room temperature for 1 h. The resulting pink precipitate was collected by centrifugation, washed with water, ethanol several times and finally dried in air.

Preparation of graphite oxide. GO was produced from natural graphite powders (universal grade, 99.985%) according to Hummers method. Firstly, natural graphite powders were treated by 5% HCl twice, then filtered, washed with distilled water thoroughly, and dried at 110°C for 24 h. Secondly, graphite powders (10 g) were placed in cold (0°C) concentrated H_2SO_4 (230 mL). KMnO_4 (30 g) was added gradually with stirring and cooling. The temperature of the solution was not allowed to go up to 20°C . The mixture was stirred for 40 min, and distilled water (460 mL) was added slowly to an increase in temperature to 98°C . The temperature was held at $35 \pm 3^\circ\text{C}$ for 30 min. Finally, distilled water (1.4 L) and 30% H_2O_2 solution (100 mL) were added after the reaction. The solution was kept at room temperature for 24 h and then the mixture was filtered, washed with 5% HCl aqueous solution until sulfate could not be detected with BaCl_2 . The reaction product was dried under vacuum at 50°C for 24 h.

Preparation of functionalized graphene sheets. The dried GO was thermally exfoliated at 300°C for 5 min under air atmosphere. The obtained samples were subsequently treated at 700°C in Ar for 3 h with a heating rate of $2^\circ\text{C}/\text{min}$.

Characterizations. The morphology of as-prepared samples was observed by a JEOL JSM-6701F field-emission scanning electron microscope (FE-SEM) at an acceleration voltage of 5.0 kV. The phase analyses of the samples were performed by X-ray diffraction (XRD) on a Rigaku-Ultima III with $\text{Cu K}\alpha$ radiation ($\lambda = 1.5418 \text{ \AA}$). Mn, Co and Ni contents were analyzed by ICP-OES (PE-3300DV) after the sample was dissolved.

Fabrication and electrochemical study on the $\text{Co}_{0.5}\text{Mn}_{0.4}\text{Ni}_{0.1}\text{C}_2\text{O}_4 \cdot n\text{H}_2\text{O}$ micropolyhedron electrode in a conventional three-electrode system. All electrochemical performances were carried out on Arbin-BT6000 electrochemical instrument in a conventional three-electrode system equipped with platinum electrode, a Hg-HgO as counter and reference electrode, respectively. Before electrochemical measurement, we have purged out O_2 from the solution by the inert gas-Ar. The working electrode was made from mixing of active materials-the $\text{Co}_{0.5}\text{Mn}_{0.4}\text{Ni}_{0.1}\text{C}_2\text{O}_4 \cdot n\text{H}_2\text{O}$ micropolyhedron electrode, acetylene black, and PTFE (polytetrafluoroethylene) with a weight ratio of 80 : 15 : 5, coating on a piece of nickel foam of about 1 cm^2 , and pressing it to a thin foil at a pressure of 5.0 MPa. The typical mass load of electrode material was 5.0 mg. The electrolyte was 3.0 M KOH solution. Galvanostatic charge-discharge methods were used to investigate capacitive properties of the $\text{Co}_{0.5}\text{Mn}_{0.4}\text{Ni}_{0.1}\text{C}_2\text{O}_4 \cdot n\text{H}_2\text{O}$ micropolyhedron electrode, which were all carried out with an Arbin-BT6000 electrochemical instrument. Cyclic voltammetry measurements of the $\text{Co}_{0.5}\text{Mn}_{0.4}\text{Ni}_{0.1}\text{C}_2\text{O}_4 \cdot n\text{H}_2\text{O}$ micropolyhedron electrode was conducted by using PARSTAT2273.

Fabrication and electrochemical study of the flexible $\text{Co}_{0.5}\text{Mn}_{0.4}\text{Ni}_{0.1}\text{C}_2\text{O}_4 \cdot n\text{H}_2\text{O}/\text{graphene}$ SASC. The PET substrates were first deposited with a layer of Pt film ($\sim 3 \times 5 \text{ nm}$ thick) and then coated with the slurry containing the active materials ($\text{Co}_{0.5}\text{Mn}_{0.4}\text{Ni}_{0.1}\text{C}_2\text{O}_4 \cdot n\text{H}_2\text{O}$ micropolyhedrons or Graphene nanosheets) *via* a similar process to that in the three electrode system and were used as the working electrode after drying. Caution: Graphene nanosheets electrode was recoated for 6 times with the above graphene slurry. The ratio of the mass of the positive electrode to that of the negative electrode is 1 : 18. In the meantime, the PVA/KOH gel electrolyte was prepared as follows: the gel electrolyte (1.52 g PVA, 2.13 g KOH, and 15 mL DI water) was prepared at 75°C for 30 min under vigorous stirring. Subsequently, two pieces of such electrodes were immersed in the PVA/KOH gel solution for 5 ~ 10 min to adsorb a layer of solid electrolyte. After the excess water was vaporized, two pieces of such electrodes containing electrolyte were pressed together on a sheet out roller. Thus, the stacked SASC was fabricated. CV measurements were carried out at 5, 10, 20, 30, 50 and $100 \text{ mV} \cdot \text{s}^{-1}$ on an electrochemical work station (PARSTAT-2273). The flexible $\text{Co}_{0.5}\text{Mn}_{0.4}\text{Ni}_{0.1}\text{C}_2\text{O}_4 \cdot n\text{H}_2\text{O}/\text{Graphene}$ SASC was galvanostatically charged and discharged at the current density of $0.5\text{--}4.0 \text{ mA} \cdot \text{cm}^{-2}$ on the Arbin-BT6000 electrochemical instrument. All the electrochemical measurements were conducted at room temperature.

- Pang, H. *et al.* The morphology evolution of nickel phosphite hexagonal polyhedrons and their primary electrochemical capacitor applications. *Part. Part. Syst. Charact.* **30**, 287–295 (2013).
- Chaikittisilp, W., Ariga, K. & Yamauchi, Y. A new family of carbon materials: synthesis of MOF-derived nanoporous carbons and their promising applications. *J. Mater. Chem. A* **1**, 14–19 (2013).
- Chaikittisilp, W. *et al.* Nanoporous carbons through direct carbonization of a zeolitic imidazolate framework for supercapacitor electrodes. *Chem. Comm.* **48**, 7259–7261 (2012).
- Hu, M. *et al.* Direct carbonization of Al-based porous coordination polymer for synthesis of nanoporous carbon. *J. Am. Chem. Soc.* **134**, 2864–2867 (2012).
- Mai, L. Q. *et al.* Hierarchical $\text{MnMoO}_4/\text{CoMoO}_4$ heterostructured nanowires with enhanced supercapacitor performance. *Nat. Commun.* **2**, 318 (2011).
- Yu, X. Z., Lu, B. G. & Xu, Z. Super long-life supercapacitors based on the construction of nanohoney comb-like strongly coupled CoMoO_4 -3D graphene hybrid electrodes. *Adv. Mater.* **7**, 1044–1051 (2014).
- Yu, Z. & Thomas, J. Energy storing electrical cables: integrating energy storage and electrical conduction. *Adv. Mater.* **26**, 4279–4285 (2014).



8. Bastakoti, B. P. *et al.* Mesoporous carbon incorporated with In₂O₃ nanoparticles as high-performance supercapacitors. *Eur. J. Inorg. Chem.* **2013**, 1109–1112 (2013).
9. Lu, X. *et al.* High energy density asymmetric quasi-solid-state supercapacitor based on porous vanadium nitride nanowire anode. *Nano Lett.* **13**, 2628–2633 (2013).
10. Lu, X. *et al.* Improving the cycling stability of metal-nitride supercapacitor electrodes with a thin carbon shell. *Adv. Energy Mater.* **4**, 1300994 (2014).
11. Niu, Z. *et al.* “skeleton/skin” strategy for preparing ultrathin free-standing singlewalled carbon nanotube/polyaniline films for high performance supercapacitor electrodes. *Energy Environ. Sci.* **5**, 8726–8733 (2012).
12. Zhou, W. *et al.* One step synthesis of Ni₃S₂ nanorod@Ni(OH)₂ nanosheet core-shell nanostructures on a three-dimensional graphene network for high-performance supercapacitors. *Energy Environ. Sci.* **6**, 2216–2221 (2013).
13. Wu, C. *et al.* Two-dimensional vanadyl phosphate ultrathin nanosheets for high energy density and flexible pseudocapacitors. *Nat. Commun.* **4**, 2431 (2013).
14. Lu, X. H. *et al.* WO_{3-x}@Au/MnO₂ core-shell nanowires on carbon fabric for high-performance flexible supercapacitors. *Adv. Mater.* **24**, 938–944 (2012).
15. Wang, X. F. *et al.* Fiber-based flexible all-solid-state asymmetric supercapacitors for integrated photodetecting system. *Angew. Chem. Int. Ed.* **53**, 1849–1853 (2014).
16. Cheng, Y. *et al.* Flexible asymmetric supercapacitors with high energy and high power density in aqueous electrolytes. *Nanoscale* **5**, 1067–1073 (2013).
17. Meng, C. Z. *et al.* Highly flexible and all-solid-state paper like polymer supercapacitors. *Nano Lett.* **10**, 4025–4031 (2010).
18. Lu, X. H. *et al.* H-TiO₂@MnO₂/H-TiO₂@C core-shell nanowires for high performance and flexible asymmetric supercapacitors. *Adv. Mater.* **25**, 267–272 (2013).
19. Wang, X. F. *et al.* Three-dimensional hierarchical GeSe₂ nanostructures for high performance flexible all-solid-state supercapacitors. *Adv. Mater.* **25**, 1479–1486 (2013).
20. Zhang, C. *et al.* Two-dimensional tin selenide nanostructures for flexible all-solid-state supercapacitors. *ACS Nano* **8**, 3761–3770 (2014).
21. Lu, X. H. *et al.* Oxygen-deficient hematite nanorods as high-performance and novel negative electrodes for flexible asymmetric supercapacitors. *Adv. Mater.* **26**, 3148–3155 (2014).
22. Yu, C. C. *et al.* A simple template-free strategy to synthesize nanoporous manganese and nickel oxides with narrow pore size distribution, and their electrochemical properties. *Adv. Funct. Mater.* **18**, 1544–1554 (2008).
23. Lei, F., Le, T. & Guo, R. Controllable preparation of NiO macrotubes from NiC₂O₄ and its application in supercapacitors. *CrystEngComm* **13**, 7246–7251 (2011).
24. Pang, H. & Chen, C. Y. Facile synthesis of cerium oxide nanostructures for rechargeable lithium battery electrode materials. *RSC Adv.* **4**, 14872–14872 (2014).
25. Pang, H. *et al.* Facile synthesis of porous nickel manganite materials and their morphology effect on electrochemical properties. *RSC Adv.* **2**, 5930–5934 (2012).
26. Wu, H. B., Pang, H. & (David) Lou, X. W. Facile synthesis of mesoporous Ni_{0.3}Co_{2.7}O₄ hierarchical structures for high-performance supercapacitors. *Energy Environ. Sci.* **6**, 3619–3626 (2013).
27. Liu, Y. Y. *et al.* Mesoporous Ni_{0.3}Co_{2.7}O₄ hierarchical structures for effective non-enzymatic glucose detection. *RSC Adv.* **4**, 33514–33519 (2014).
28. Pang, H. *et al.* Facile synthesis of porous ZnO-NiO composite micropolyhedrons and their application for high power supercapacitor electrode materials. *Dalton Trans.* **41**, 13284–13291 (2012).
29. Yuan, C. Z. *et al.* Green template-free synthesis of mesoporous ternary Co-Ni-Mn oxide nanowires towards high-performance electrochemical capacitors. *Part. Syst. Charact.* DOI:10.1002/ppsc.201300333 (2014).
30. Jung, I., Choi, J. & Tak, Y. Nickel oxalate nanostructures for supercapacitors. *J. Mater. Chem.* **20**, 6164–6169 (2010).
31. Cheng, G. H. *et al.* Anodization driven synthesis of nickel oxalate nanostructures with excellent performance for asymmetric supercapacitors. *J. Mater. Chem. A* DOI:10.1039/c4ta03648d (2014).
32. Ren, J. *et al.* Twisting carbon nanotube fibers for both wire-shaped micro-supercapacitor and micro-Battery. *Adv. Mater.* **25**, 1155–1159 (2013).
33. Choi, B. G. *et al.* High performance of a solid-state flexible asymmetric supercapacitor based on graphene films. *Nanoscale* **4**, 4983–4988 (2012).
34. Lei, Z. B., Zhang, J. T. & Zhao, X. S. Ultrathin MnO₂ nanofibers grown on graphitic carbon spheres as high-performance asymmetric supercapacitor electrodes. *J. Mater. Chem.* **22**, 153–160 (2012).
35. El-Kady, M. F., Strong, V., Dubin, S. & Kaner, R. B. Laser scribing of high-performance and flexible graphene-based electrochemical capacitors. *Science* **335**, 1326–1330 (2012).
36. Lu, X. H. *et al.* Stabilized TiN nanowire arrays for high-performance and flexible supercapacitors. *Nano Lett.* **12**, 5376–5381 (2012).
37. Yang, P. *et al.* Hydrogenated ZnO core-shell nanocables for flexible supercapacitors and self-powered systems. *ACS Nano* **7**, 2617–2626 (2013).
38. Xiao, X. *et al.* Freestanding mesoporous VN/CNT hybrid electrodes for flexible all-solid-state supercapacitors. *Adv. Mater.* **25**, 5091–5097 (2013).
39. Zilong, W., Zhu, Z., Qiu, J. & Yang, S. High performance flexible solid-state asymmetric supercapacitors from MnO₂/ZnO core-shell nanorods/specially reduced graphene oxide. *J. Mater. Chem. C* **2**, 1331–1336 (2014).
40. Gao, L. N. *et al.* Efficient synthesis of hierarchical NiO nanosheets for high-performance flexible all-solid-state supercapacitors. *J. Mater. Chem. A* **1**, 7168–7173 (2013).
41. Dong, X. L. Flexible and wire-shaped micro-supercapacitor based on Ni(OH)₂-nanowire and ordered mesoporous carbon electrodes. *Adv. Funct. Mater.* **24**, 3405–3412 (2014).
42. Yu, D. S. Scalable synthesis of hierarchically structured carbon nanotube-graphene fibres for capacitive energy storage. *Nat. Nanotechnol.* **9**, 555–562 (2014).

Acknowledgments

We acknowledge financial support from the National Key Basic Research Program of China (973 Program, 2014CB648300), the Program for New Century Excellent Talents in University (grant no. NCET-13-0645, NCET-13-0872), the National Natural Science Foundation of China (21201010, 21422402, 20904024, 51173081, 61136003, 61106036, and U1304504), the Program for Innovative Research Team (in Science and Technology) in University of Henan Province (14IRTSTHN004), the Science & Technology Foundation of Henan Province (122102210253, 13A150019, 14B150001 and 14A430038), the Natural Science Foundation of Jiangsu Province (BM2012010, BK20140060, BK20130037), Specialized Research Fund for the Doctoral Program of Higher Education (20133223110008), the Program for Graduate Students Research and Innovation of Jiangsu Province (CXZZ12-0454), the China Postdoctoral Science Foundation (2012M521115), the Ministry of Education of China (IRT1148), the Priority Academic Program Development of Jiangsu Higher Education Institutions (PAPD), the Six Talent Plan (2012XCL035) and Qing Lan Project of Jiangsu Province and the Opening Research Foundations of the State Key Laboratory of Coordination Chemistry (Nanjing University).

Author contributions

Y.Z.Z., J.H.Z., J.X., L.L.W., H.G.F. and H.P. conceived and designed the experiments. Y.Z.Z., W.Y.L., H.P. and W.H. analyzed the measurements. H.P. wrote the manuscript in collaboration with all the authors.

Additional information

Supplementary information accompanies this paper at <http://www.nature.com/scientificreports>

Competing financial interests: The authors declare no competing financial interests.

How to cite this article: Zhang, Y.-Z. *et al.* Room temperature synthesis of cobalt-manganese-nickel oxalates micropolyhedrons for high-performance flexible electrochemical energy storage device. *Sci. Rep.* **5**, 8536; DOI:10.1038/srep08536 (2015).



This work is licensed under a Creative Commons Attribution 4.0 International License. The images or other third party material in this article are included in the article's Creative Commons license, unless indicated otherwise in the credit line; if the material is not included under the Creative Commons license, users will need to obtain permission from the license holder in order to reproduce the material. To view a copy of this license, visit <http://creativecommons.org/licenses/by/4.0/>